Electronic Supplementary Information

Probing mechanical properties and failure mechanisms of fibrils of self-assembling peptides

Federico Fontana[a] and Fabrizio Gelain [*a,b]

[a.] *Fondazione IRCCS Casa Sollievo della Sofferenza, Unità Ingegneria Tissutale, Viale Cappuccini 1, San Giovanni Rotondo, 71013 Foggia, Italy*

[b.] *Center for Nanomedicine and Tissue Engineering (CNTE), ASST Ospedale Metropolitano Niguarda, Piazza dell'Ospedale Maggiore 3, 20162 Milan, Italy*

Material and Methods

1.1. Self-assembling simulations of $(LDLK)_3$ and FAQ-$(LDLK)_3$ peptides

All-trans configuration of $(LDLK)_3$ and FAQ-$(LDLK)_3$ peptides were generated by Pymol (https://pymol.org) and mapped according to the MARTINI model. The C- and N- terminal of peptide monomers were acetylated and amidate respectively. At neutral pH, arginine, lysine and aspartic acid side chains, because of their weak basic and acidic nature, can be considered fully protonated and deprotonated respectively. Peptides have been randomly distributed in explicit water cubic boxes built by using PACKMOL in order to have the correct spatial distribution of the monomers [1]. Atoms belonging to different peptides were placed at minimum distance of 10 Å far from each other (see **Table S1** for details). In MARTINI coarse-grained molecular dynamics (CG-MD) simulations it is necessary to define peptide secondary structures, and the above mentioned parameters, to which individual amino acid residue must evolve[2]. The secondary structures have been assigned as shown in **Table S1**, according to the evidences obtained from previous experimental analyses [3] and from ssNMR spectra as shown in Fig. S14. (See Section 1.8 for ssNMR experiment details) MD simulations were performed using the version 4.5.5 of GROMACS package [4]. Prior to the production phase, the systems underwent to an equilibration phase (a 3000-steps minimization using steepest descents method) in order to eliminate high-energy interactions. The production phase was conducted in the NPT ensemble. Solutes and solvent were coupled independently to an external bath (T = 298 K) with a coupling constant (τT) of 1 ps using v-rescale thermostat. Periodic boundary conditions were imposed, and pressure was maintained at 1 bar using the Berendsen coupling [5]. The isothermal compressibility was set at $3 * 10^{-4}$ bar^{-1} and the coupling constant (τP) was 1 ps. The constraints on lengths and angles of the bonds were applied with the LINCS algorithm. All systems were simulated as indicated in **Table S1** using an integration time-step of 20 fs, while snapshots of individual trajectories were saved every 100 fs.

1.2. Self-assembling simulations of FAQ peptides

Due to the lack of accurate structural information about FAQ peptides, the self-assembly process of this SAP class has been investigated by means of more accurate UA-MD simulations. The simulation details of FAQ-derived SAPs are shown in **Table S2**. Peptide monomers have the C-terminus amidated and the N-terminus acetylated. Arginine residues are in the protonated state. Extended conformations of monomers were built with Pymol software by imposing all-trans geometry on the backbone dihedrals (https://pymol.org). The monomers in extended conformation have been embedded in a box of explicit water and submitted to three simulations of 50 ns/each with different initial velocity distributions. A distance of 10 Å has been left between

the peptide and the box edges to preserve the minimum image convention. On the obtained conformational sampling, a cluster analysis has been performed by means of the gromos algorithm of Daura [6]. The centrotypes of the first cluster were used to prepare systems containing eight monomers: each system was composed by centrotypes picked up in relative amount needed to achieve 70–80% representation degree of the monomeric sampling. The initial configurations of the multipeptide systems were prepared by insertion of the selected centrotypes in random orientations and positions in cubic boxes filled by explicit water and so that atoms belonging to different peptides were at least 10 Å away from each other [1].
Molecular dynamics were run using version 4.5.5 of the GROMACS simulation package and the GROMOS53a6 force field [3][7]. Prior to the production phase, the systems underwent to an equilibration phase consisting in the following steps: steepest descent minimization first in vacuum then in water and ions, a brief simulation in NVT ensemble with 2 fs time-step, position restrained peptides and the temperature fixed at 298 K. The production phase was conducted in the NPT ensemble. Solutes and solvent were coupled independently to an external bath (T = 298 K) with a coupling constant (τT) of 0.1 ps using v-rescale thermostat. Periodic boundary conditions were imposed, and pressure was maintained at 1 bar using the Berendsen coupling [5]. The isothermal compressibility was set at $4.5*10^{-5}$ bar^{-1} and the coupling constant (τP) was 0.1 ps. The constraints on lengths and angles of the bonds were applied with the LINCS algorithm. All systems were simulated as indicated in **Table S2** using an integration time-step of 2 fs, while snapshots of individual trajectories were saved every 10 fs.

1.3. UA Steered molecular dynamics simulations of $(LDLK)_3$ and FAQ-$(LDLK)_3$ peptides

The initial conformations of the systems have been obtained through back-mapping procedure of the resulting structures from CG-MD simulations (See **Fig.1, Fig. S1, Fig. S2, Fig. S7, Fig. S8**). At the neutral pH, lysine and arginine and aspartic acid side chains, because of their weak basic and acidic nature, can be considered fully protonated and deprotonated respectively. Steered molecular dynamics simulations were run using the version 2016.3 of the GROMACS simulation package [9], using two GTX 1080 GPUs. Two set of UA-SMD, named axial stretching and bending, have been conducted using the Gromos53a6 force-field [7]. Prior to the production phase, the systems underwent to an equilibration phase consisting in the following steps: steepest descent minimization first in vacuum then in water and ions, a brief simulation in NVT ensemble with a 2 fs time-step, position restrained peptides and the temperature fixed at 298 K. Then a 200 ps long simulation in NVE ensemble, with position restrained peptides has been conducted in order to optimize the charge side-chains orientations. The production phase was conducted in the NVE ensemble. In axial stretching scenario, one end of the fibril (seed) structure has been fixed by constraining the motion of Cα-atoms at the bottom strand of the sheets. The other end of the fibril was deformed by axial loading. Instead, in bending scenario the unrestrained end was deformed by lateral loading. The boundary conditions consisted of fixing Cα-atoms on the top and bottom strands with a SMD spring constant equal to 1000 $kJ*mol^{-1}nm^2$ and a displacement rate of 0.01 nm/ps [8]. Each system was simulated in explicit water box and submitted to five production runs differing for the initial velocity distribution, as shown in **Table S3**. The constraints on lengths and angles of the bonds were applied with the LINCS algorithm. All systems were simulated as indicated in **Table S3** using an integration time-step of 2 fs, while the snapshots and the measures of force/displacement of individual trajectories were saved every 10 fs.

1.4. CG Steered molecular dynamics simulations of $(LDLK)_3$ and FAQ-$(LDLK)_3$ peptides

The initial conformations of the systems were obtained through back-mapping procedure of the resulting structure from CG-MD simulations (See **Fig.1, Fig. S1, Fig. S2, Fig. S7, Fig. S8**). CG-SMD simulations were run using the version 2016.3 of the GROMACS simulation package, using two GTX 1080 GPUs [9]. Two set of CG-SMD, analogues to UA-SMD simulations, have been conducted using the GoMARTINI force-field [10].
In GoMARTINI CG-MD simulations, it has been necessary to define peptide secondary structures through Lennard-Jones interactions based on the contact map of native fibril (seed). The Lennard-Jones potential is defined as follows:

$$U_{LJ} = 4\epsilon_{ij}\left[\left(\frac{\sigma}{r}\right)^{12} - \left(\frac{\sigma}{r}\right)^{6}\right]$$

In GoMARTINI model, ε_{ij} is usually set to a larger value than in MARTINI force-field and represents the strength of the hydrogen bonds and other contribution such as ionic briges. Indeed, the parameter ε_{ij} is expressed in unit of ε = 6.276 Kj/mol^{-1}. Then, the parameter λ in the native contact energy, $\varepsilon_{ij} = \lambda\ \varepsilon$, is a tunable parameter of the GoMARTINI model, whose optimum value can be found to match quantitatively the GoMARTINI and UA model [10]. To reproduce the tendencies observed in UA-SMD, the value of λ was set to 0.5. Prior to the production phase, the systems underwent to an equilibration phase consisting in the following steps: steepest descent minimization first in vacuum then in water and ions, a brief simulation in NVT ensemble with 0.002 ps time-step, position restrained peptides and the temperature fixed at 298 K. Then a 200 ps long simulation in NVE ensemble, with position restrained peptides has been conducted in order to optimize the charge side-chains orientations. The production phase was conducted in the NVE ensemble. In axial stretching scenario, one end of the fibril (seed) structure has been fixed by constraining the motion of backbone grains at the bottom strand of the sheets. The other end of the fibril was deformed by axial loading. Instead, in bending scenario the unrestrained end was deformed by lateral loading. The boundary conditions consisted of fixing backbone grains on the top and bottom strands with an SMD spring constant equal to 1000 kJ*mol^{-1}nm^2 and a displacement rate of 0.01 nm/ps [8][10]. Each system was simulated in explicit water box and submitted to five different simulations, as shown in **Table S4.** The constraints on lengths and angles of the bonds were applied with the LINCS algorithm. All systems were simulated as indicated in **Table S4** using an integration time-step of 2 fs, while the snapshots and the measures of force/displacement of individual trajectories were saved every 10 fs.

1.5. Analysis of SMD simulations

The cross-sectional area of each fibril (or seed) has been approximated to a rectangle, whose sides are defined by two segments; the first segment joining the center of mass of two β-strands, the second segment joining the N- and C- terminus of peptides belonging to one end of the fibrils, as shown in the following scheme.

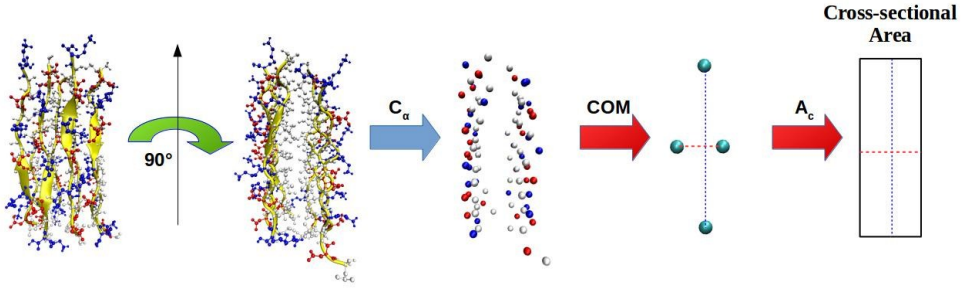

Scheme 1. Calculation of the cross-sectional area (A_c)

The stress-strain curves were obtained by converting the force-displacement curves. Stress values were derived by dividing the force values for the cross-sectional area, according to the following formula:

$$\sigma(t) = F^{(t)}/A_c$$

Where F(t) indicates the value of the force obtained from SMD, A_c indicates the measure of the cross-sectional area.

The engineering strain curves were obtained from the displacement curves through the following formula:

$$\epsilon(t) = \frac{L(t) - L_0}{L_0}$$

Where L(t) indicate the measure of the displacement at a given time-step, L_0 indicates the starting length of the structures.
Young's modulus and Shear modulus have been derived by measuring the slope of the stress-strain curves.
The distribution of strains within fibrils (or seeds) has been calculated through the formula of shear contribution ratio [11]:

$$s(L) = \frac{1Eh^2}{4GL^2}$$

If s(L) > 1 → non-covalent interactions (i.e. hydrogen bonds) are being shared (pulled orthogonal to the bonding direction)
If s(L) < 1 → non-covalent interactions (i.e. hydrogen bonds) are stretched in tension (pulled in the bonding direction)

1.6 Measures of the performance GoMARTINI vs Gromos53a6

For each simulation setup, the production parameters have been measured in terms of simulated time ns/day, as shown in **Table S10** and **Table S11.** The results are in agreement with the main results of the recent work of Biagini and co-workers [9].

1.7 Morphoscanner Analysis

As reported by Saracino et al. [12] the input parameters of Morphoscanner were set equal to the number of peptides (S) and of backbone grains (or Cα atoms in the UA model) (SL). Then, S was set equal to 8 for the analysis of fibril seed simulations (Fig. 1-2), whereas S was set equal to 100 for the analysis of fibril simulations (Fig. 3-4). Instead, SL was set equal to 10, 12 and 22 for the analysis of FAQ, $(LDLK)_3$ and FAQ-$(LDLK)_3$ MD simulations respectively. The organization of the systems over time was schematized into a count of the total β-interactions in the systems. β-interactions were set to 1 when distance between backbone atom-groups (grains) or Cα atoms fall between 4.7 and 5.3 Å. In addition, the shift profiles were used to track peptides preferential arrangement during self-assembling.

1.8 Hydrogel preparation and ssNMR characterization at natural abundance

In order to elucidate supramolecular organization of peptide hydrogels, ssNMR experiments were performed with solid-phase synthesized peptides. Solid-state NMR (ssNMR) provided atomic-level structural information about hydrogels organization. This allowed to derive secondary structure information at residue-level from the so-called 'secondary chemical shifts'.

The $(LDLK)_3$ and FAQ-$(LDLK)_3$ hydrogels were prepared by dissolving purified peptide powder at a concentration of 1% (w/v) in distilled water, sonicated for 30 min, and incubated at 4 °C for 24h, a day prior the ssNMR characterization. The rigid fractions of the self-assembling peptides were quantified using one-dimensional (1D), so-called dipolar NMR experiments (i.e. experiments that rely on the presence of dipolar couplings between ^{1}H and ^{13}C). NMR experiments were performed without synthetic ^{13}C-isotope enrichment. All ^{13}C-detected CP experiments were initially optimised on ^{13}C-labelled histidine and by using a ^{1}H to ^{13}C CP magnetization transfer-time of 1 ms for all samples: the obtained parameters were used for the hydrogels without further optimisation. The spectra were acquired at 700 MHz magnetic field and 15 kHz magic angle spinning (MAS) and 278 K sample temperature.

Figures

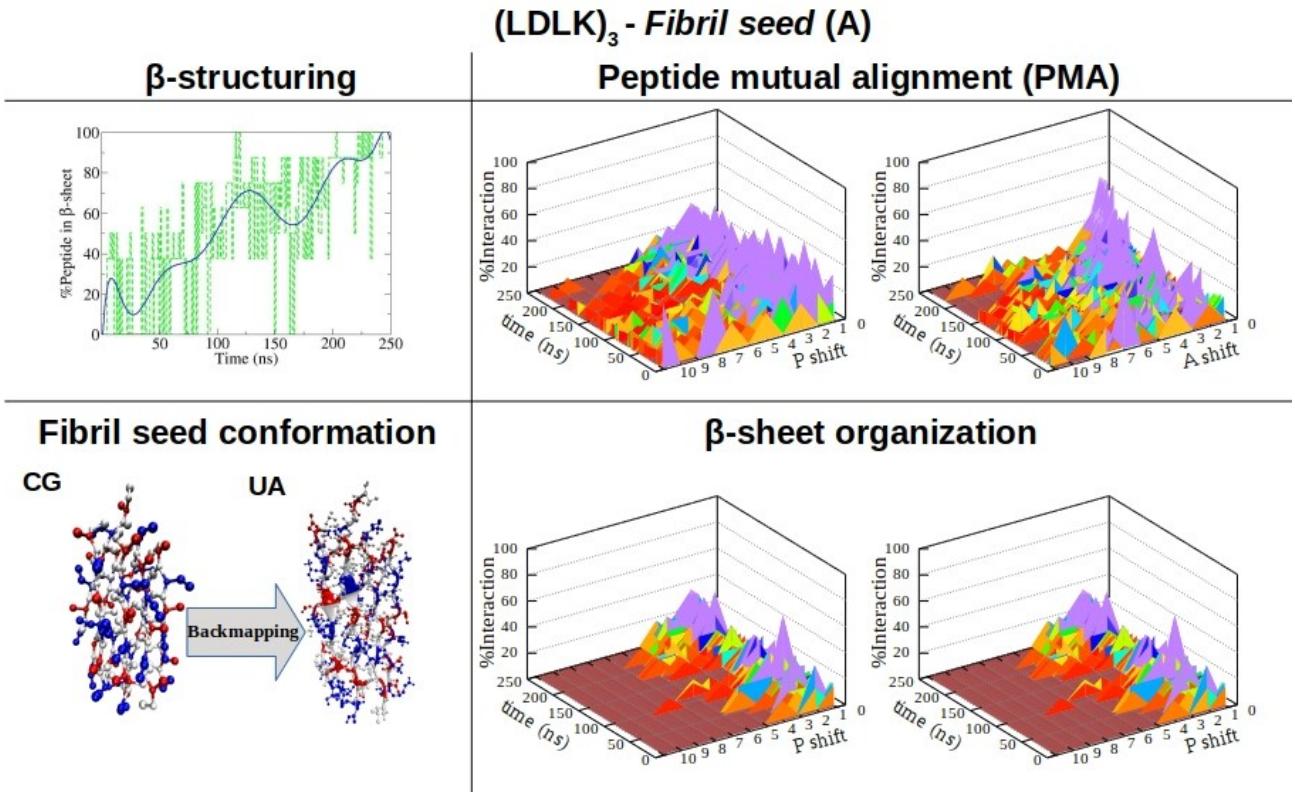

Fig. S1. Shift profiles and β-structuring propensity of $(LDLK)_3$ SAPs. P refers to the parallel alignment, A refers to the antiparallel alignment. Differently from the data shown in Fig.1, $(LDLK)_3$ SAPs assembled in a less ordered double layered β-sheet structure. Indeed, $(LDLK)_3$ were preferentially antiparallel aligned, whereas β-strands didn't show any preferential alignment.

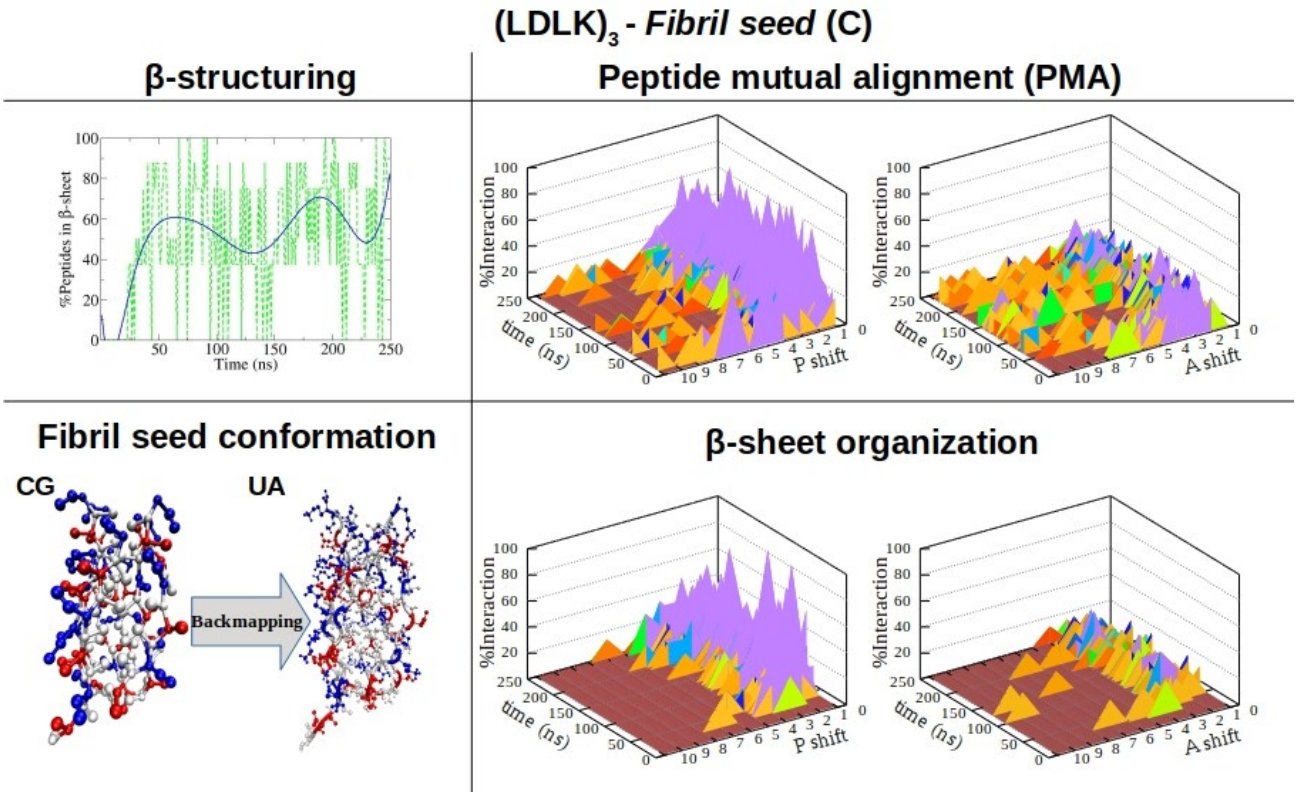

Fig. S2. Shift profiles and β-structuring propensity of $(LDLK)_3$ SAPs. P refers to parallel alignment, A refers to antiparallel alignment. Differently from the data shown in Fig.1, $(LDLK)_3$ SAPs assembled in a less ordered double layered β-sheet structure. Indeed, $(LDLK)_3$ peptides were preferentially parallel aligned, such as β-strands.

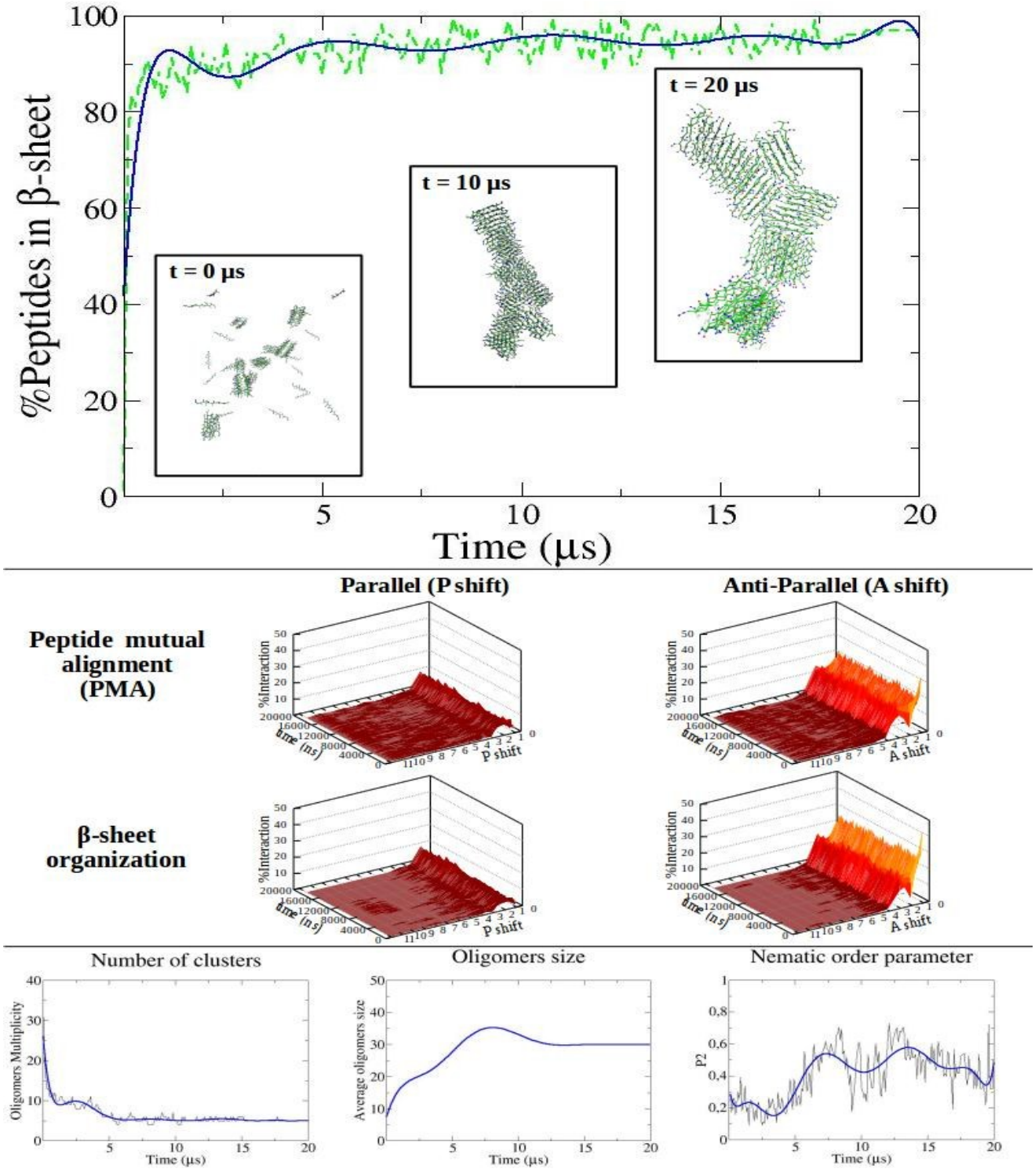

Fig. S3. ONE-POT CG-MD of $(LDLK)_3$ SAPs. ONE-POT CG-MD simulations have been prepared according to the data reported in TableS1. The fibril seed conformation corresponded to the final structure of CG-MD simulation reported in Fig. 1a. The $(LDLK)_3$ SAPs, such as β-strands were mutually antiparallel aligned. This tendency was also reflected by nematic order parameter, which reached value equal to 0.5 within 5 μs.

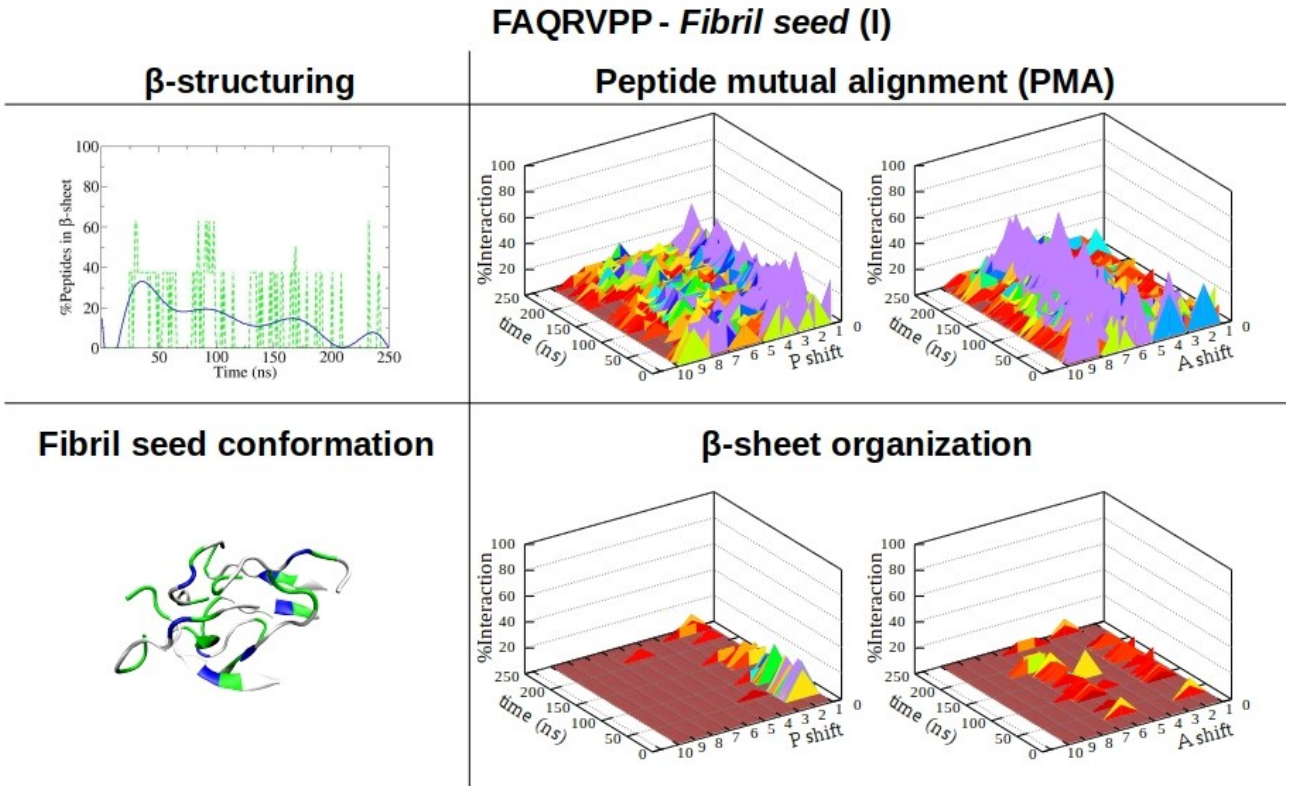

Fig. S4. Shift profiles and β-structuring propensity of FAQ SAPs, 1st replica. FAQ peptides didn't show any preferential mutual alignment. This tendency is also reflected in β-sheet organization. Such features were due to the "β-breaker" effect of Pro residues.

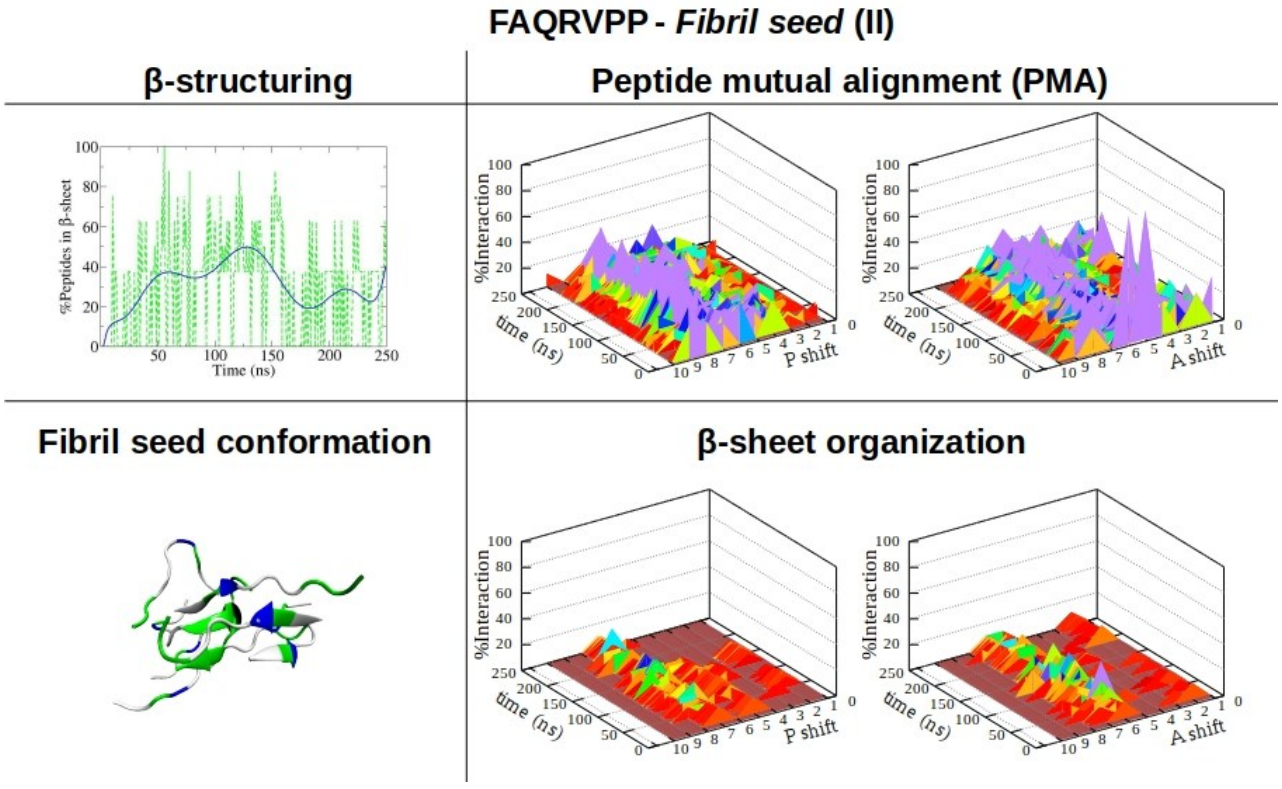

Fig. S5. Shift profiles and β-structuring propensity of FAQ SAPs, 2nd replica. As shown in Fig. S4, FAQ peptides didn't show any preferential mutual alignment. However, β-strands were weakly aligned according to antiparallel and parallel arrangement.

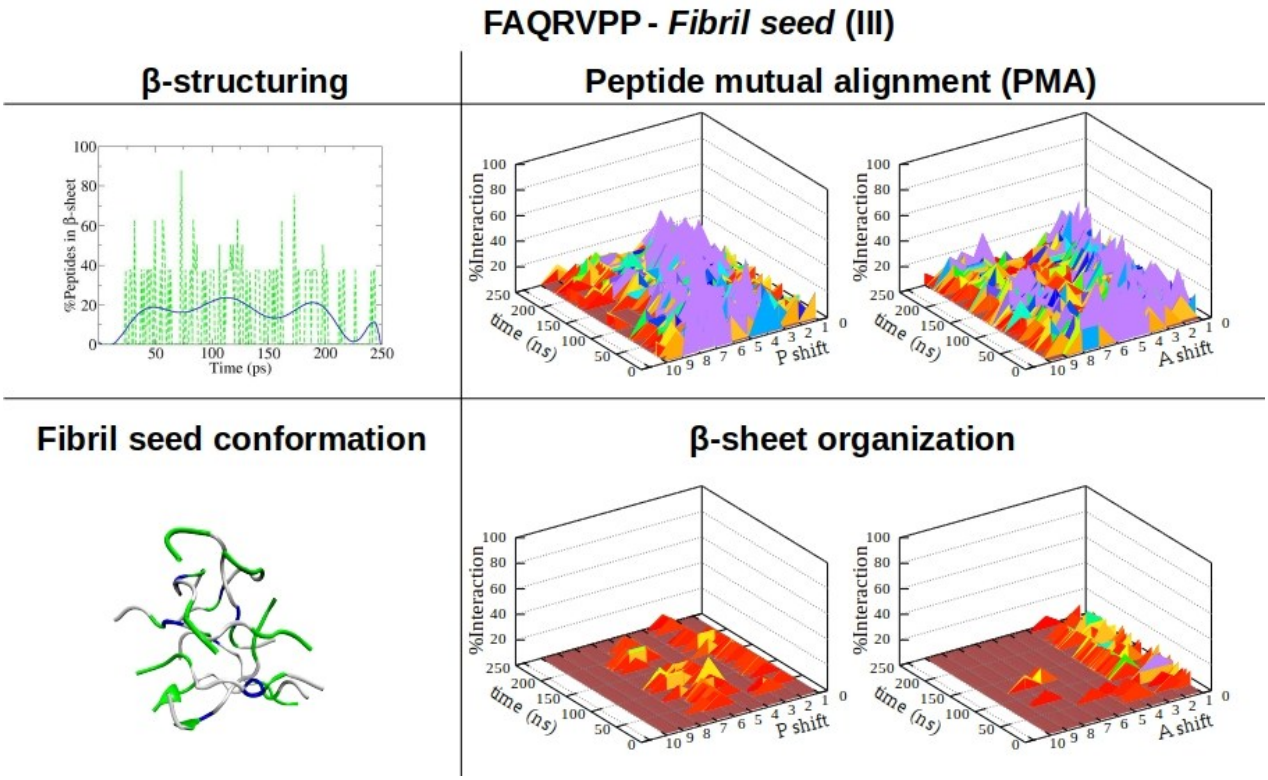

Fig. S6. Shift profiles and β-structuring propensity of FAQ SAPs, 3rd replica. As shown in Fig. S4, the FAQ peptides didn't show any preferential mutual alignment and any β-strands alignment.

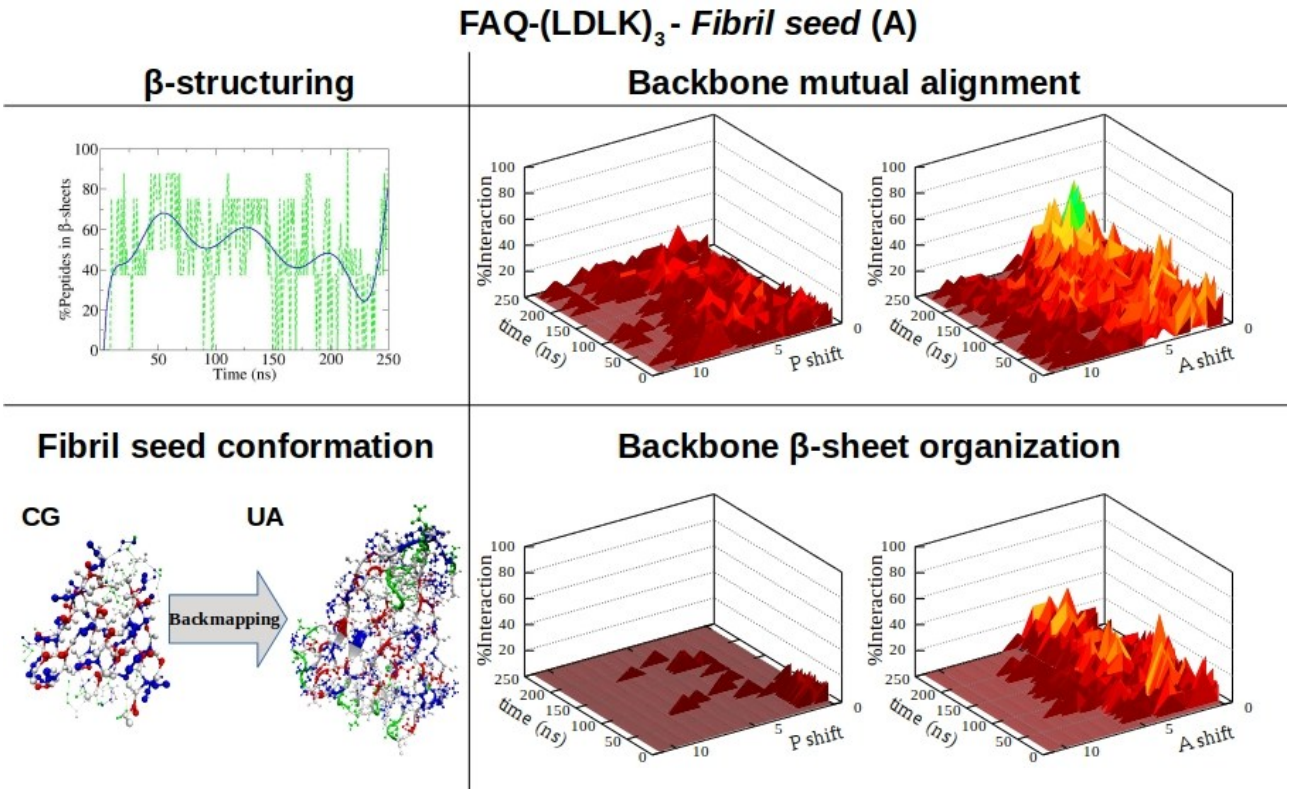

Fig. S7. Shift profiles and β-structuring propensity of backbone moieties FAQ-$(LDLK)_3$ SAPs. As shown in Fig. 1b, FAQ-$(LDLK)_3$ backbone moieties PMA and β-sheet organization reflected those of $(LDLK)_3$ SAPs. Due to the presence of FAQ functional motif, FAQ-$(LDLK)_3$ peptides assembled into disordered aggregates.

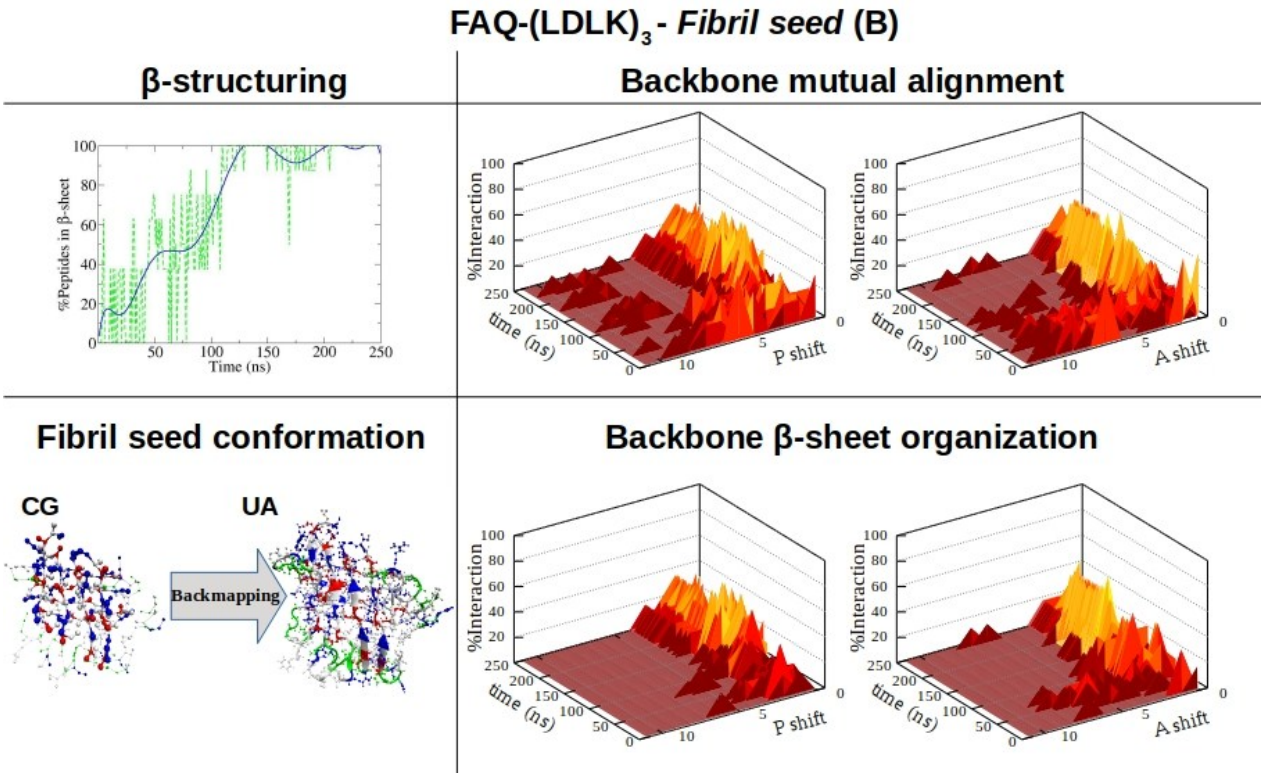

Fig. S8. Shift profiles and β-structuring propensity of backbone moieties FAQ-$(LDLK)_3$ SAPs. Differently from the results shown in Fig. 1B and Fig. S7, FAQ-$(LDLK)_3$ assembled into two orthogonally oriented β-sheets. However, the β-strands organization reflected the backbone moieties mutual alignment. Indeed, peptides are mutually alignment both in A and P.

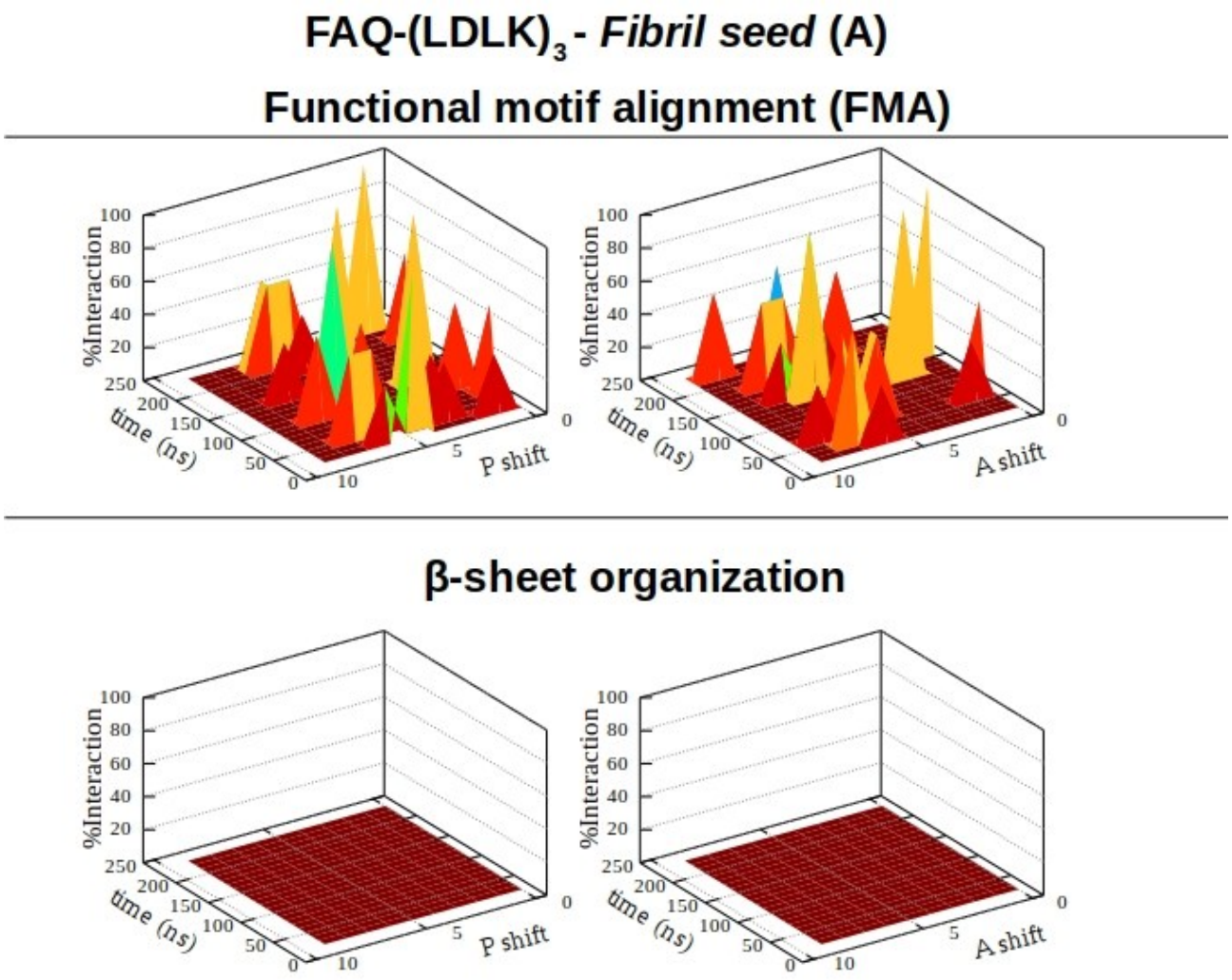

Fig. S9. Shift profiles and β-structuring propensity of functional motif FAQ-$(LDLK)_3$ SAPs. According to the data shown in Fig. S4, Fig. S5 and Fig. S6, FAQ functional motifs didn't assemble into ordered aggregates. This hampered the formation of β-sheet structures. Such features didn't alter the β-structuring propensity of backbone moieties, as shown in **Fig. S7**.

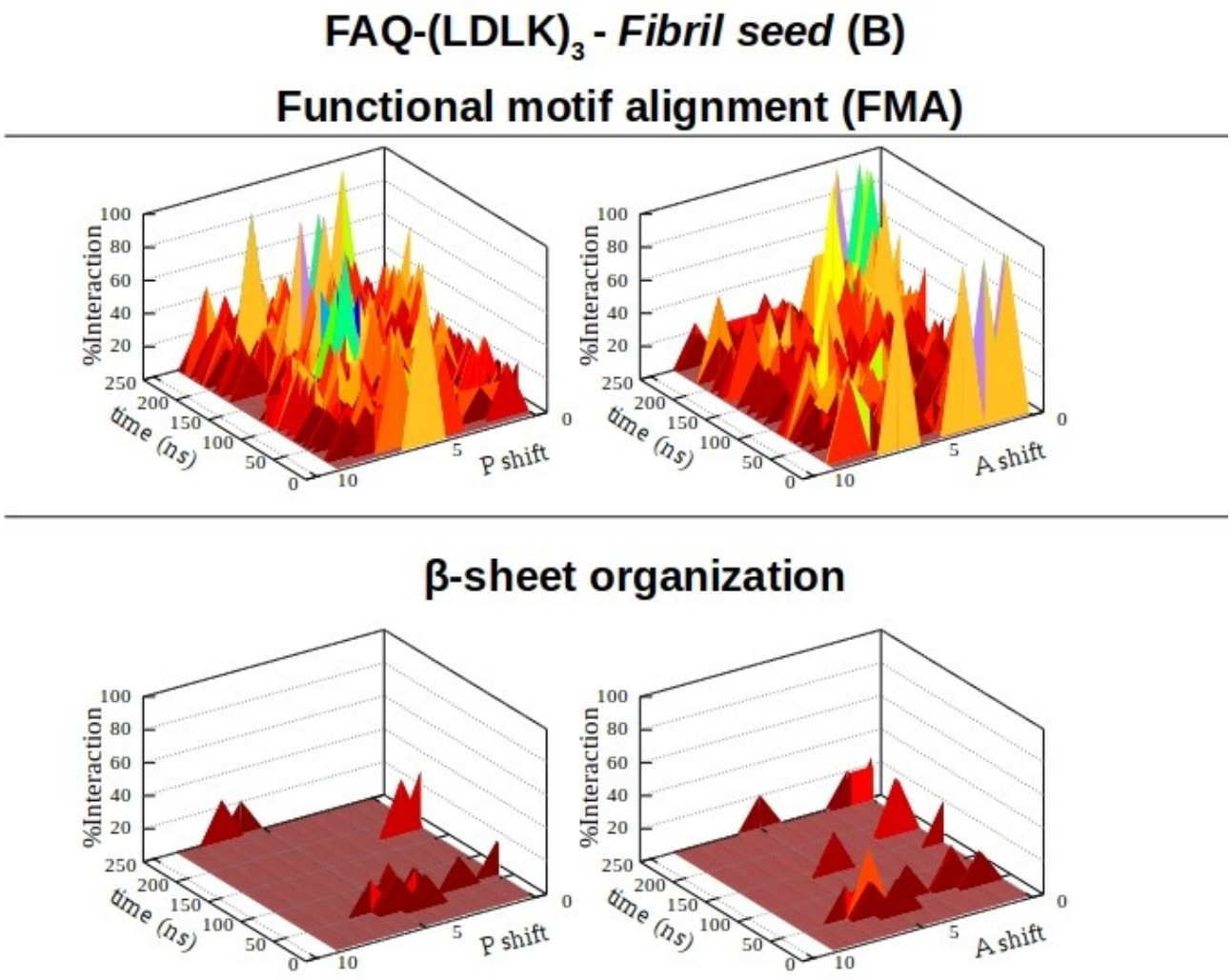

Fig. S10. Shift profiles and β-structuring propensity of functional motif FAQ-$(LDLK)_3$ SAPs. According to the data shown in Fig. S4, Fig. S5 and Fig. S6, FAQ functional motif didn't assemble into ordered aggregates. However, FAQ functional motifs assembled into disordered β-sheet structures. Such features heavily altered the β-structuring propensity and mutual alignment of backbone moieties, as shown in **Fig. S8**.

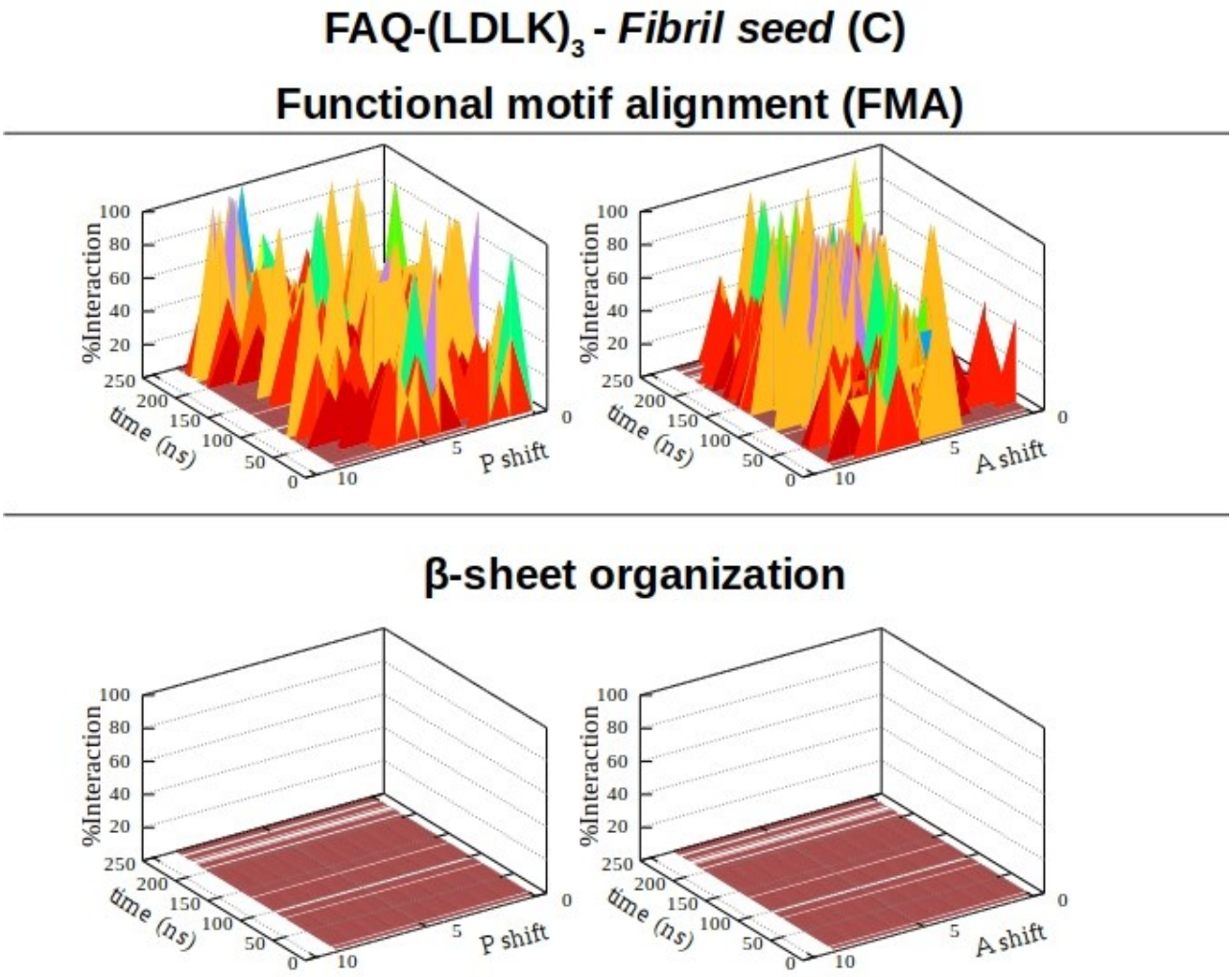

Fig. S11. Shift profiles and β-structuring propensity of functional motif FAQ-$(LDLK)_3$ SAPs. According to the data shown in Fig. S4, Fig. S5 and Fig. S6, FAQ functional motif didn't assemble into ordered aggregates. This hampered the formation of β-sheet structures. Such features didn't alter the β-structuring propensity of backbone moieties, as shown in **Fig. 1b**.

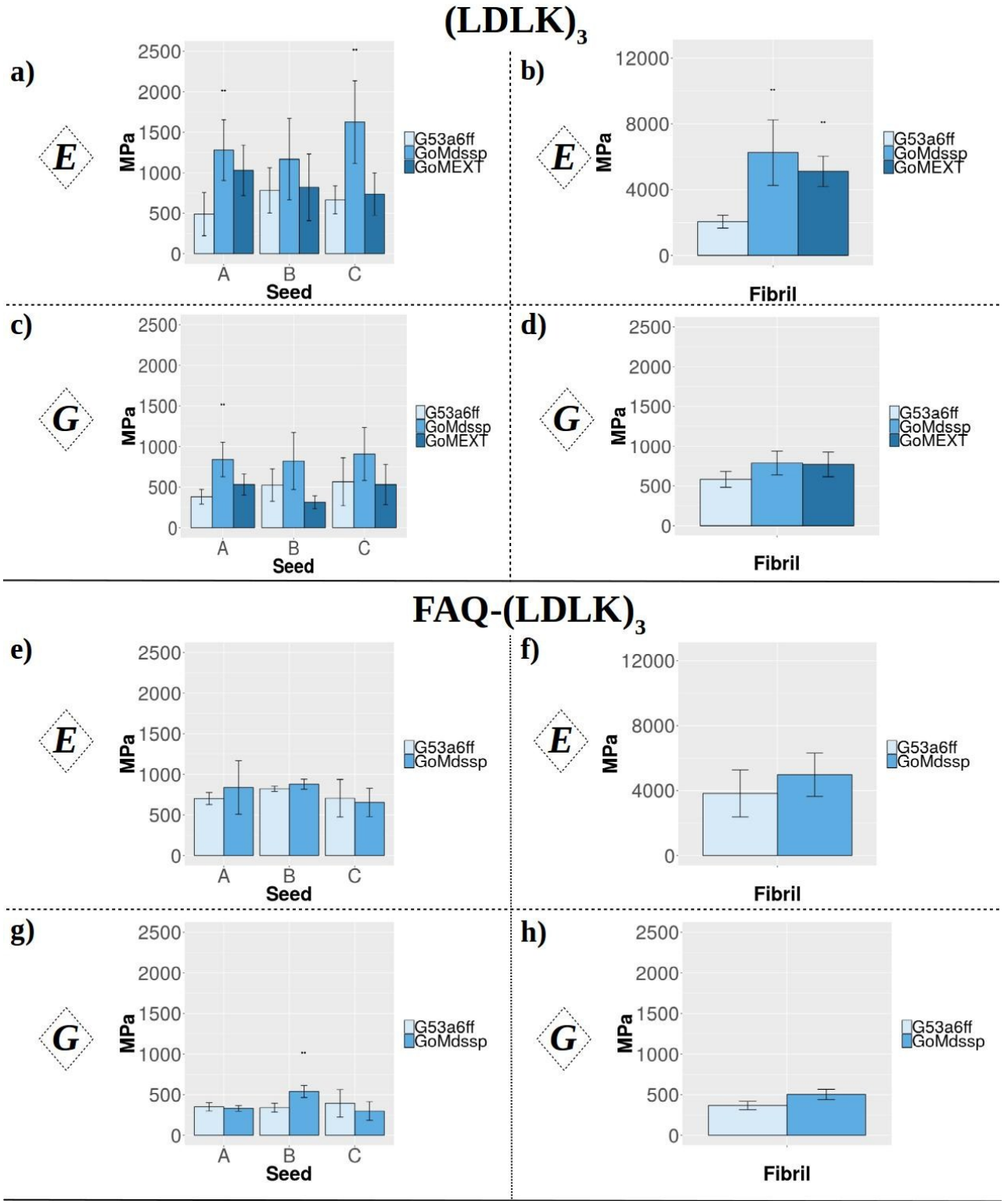

Fig. S12. Statistical analysis of Young's and Shear Moduli. G53a6ff refers to the UA-SMD approach. GoMdssp refers to the CG-SMD approach with SS parameters assigned as shown in Table S5 and S7- GoMEXT refers to CG-SMD approach with SS parameters assigned as shown in Table S6. E refers to the Young's Modulus and G to the shear modulus. The GoMdssp approach provided similar results to G53a6ff approach.

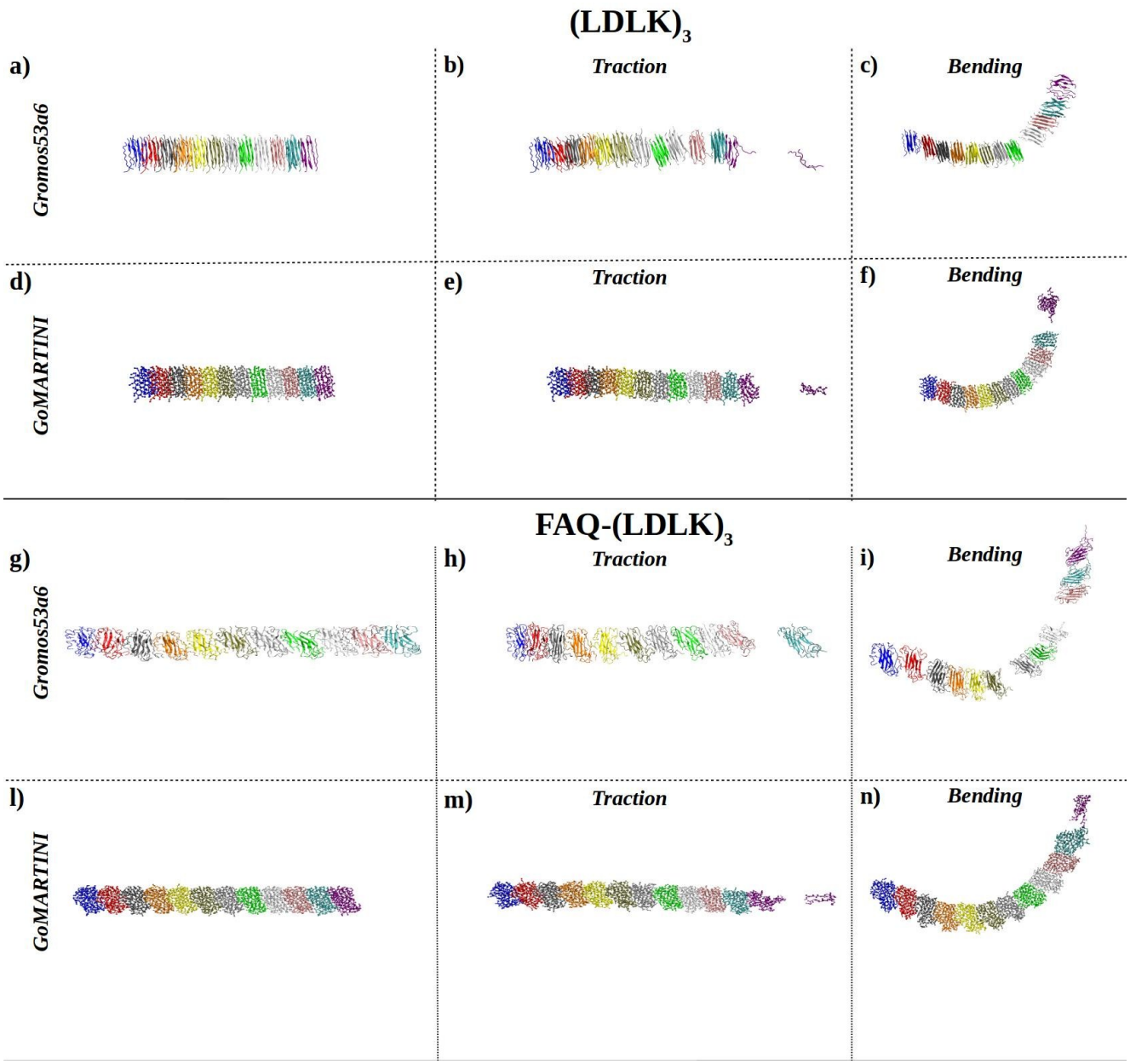

Fig. S13. Graphical representation of failure mechanism of SAPs fibrils. Gromos53a6 refers to the UA-SMD approach, whereas GoMARTINI refers to the CG-SMD setup. The $(LDLK)_3$ and FAQ-$(LDLK)_3$ fibril structures have been built by stacking fibril seed structures, which are highlighted by different colors. In UA-SMD (**b**) and CG-SMD axial stretching simulations (**e)** the $(LDLK)_3$ fibrils shown similar failure mechanisms, which involved the displacement of two β-strands belonging to the un-restrained end of the models (as depicted in **a** and **d**). By analyzing bending UA-SMD (**a**) and CG-SMD (**f**) simulation of $(LDLK)_3$ fibrils, it has been possible to observe little differences in the failure mechanisms. Indeed, the failure rupture points don't correspond to fibril seed contact-point. The same conclusion can be addressed also for FAQ-$(LDLK)_3$ fibrils, by visual inspection of failure structures reported in h), i), m) and n).

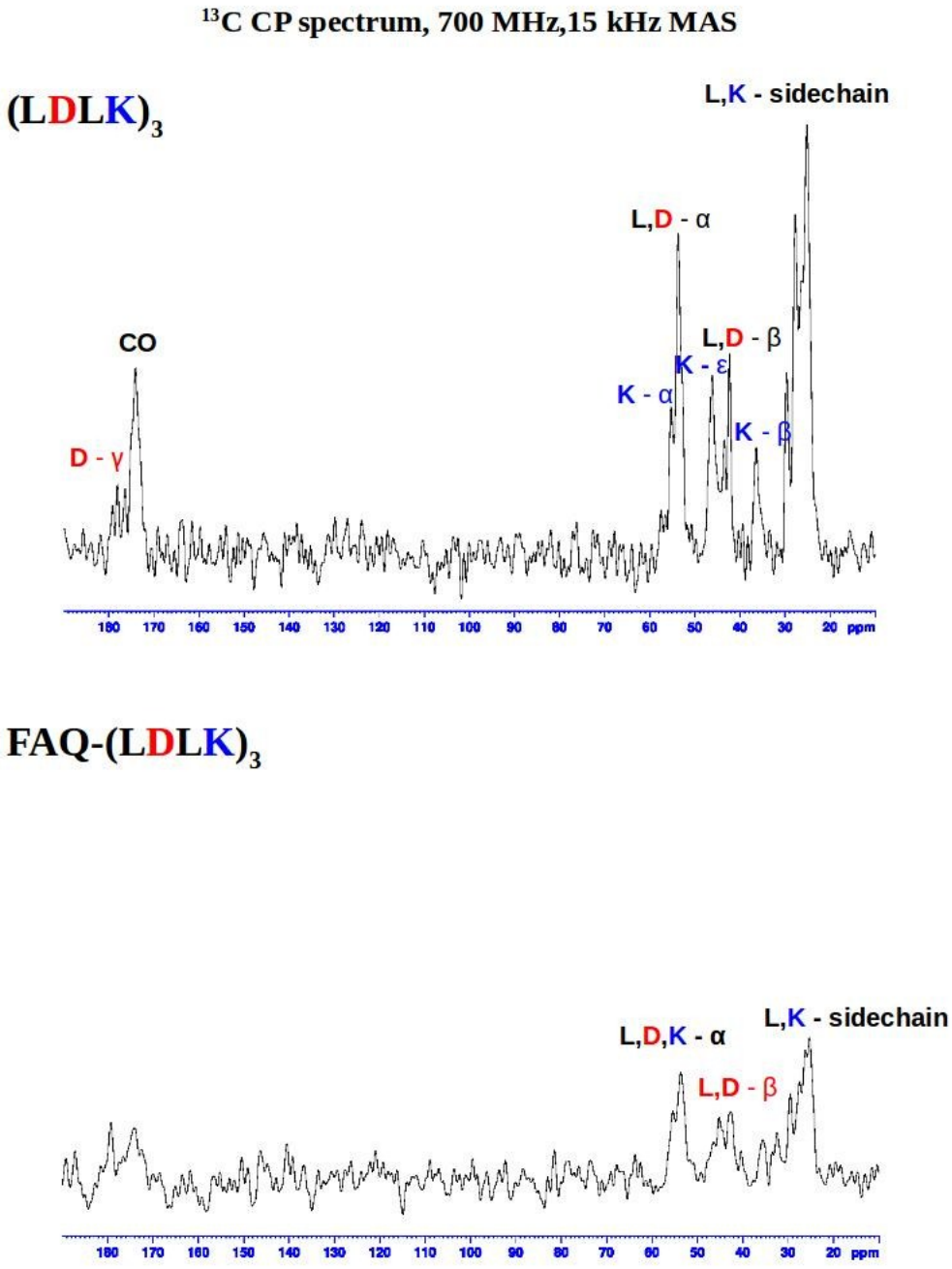

Fig. S14. ^{13}C-detected dipolar cross-polarization ssNMR spectra: characterization of the immobile fraction of the hydrogels. The ssNMR spectra showed that $(LDLK)_3$ SAPs were fully assembled, completely rigid, and β-structured. Indeed, the chemical shifts corresponding to β-strand conformation were easily identified. [13] Instead, the FAQ-$(LDLK)_3$ SAPs showed a lower rigidity at the nanoscale level. However, the chemical shift pointed out that $(LDLK)_3$ moieties assembled in rigid and β-structured aggregates. Such information has been used to assign secondary structure parameters in GoMARTINI simulations.[10]. See Section 1.8 for details about hydrogels preparation and ssNMR characterization.

Tables

Sequence ID	Sequence	Box size (nm)	CG ions beads (NA+/CL-)	CG Water beads	N° of peptides + N° of seed (8-mer)	N° of sim x time (ns)
$(LDLK)_3$	**LDLKLDLKLDLK**	12.39	0/0	15829	8	3 x 250
$(LDLK)_3$	**LDLKLDLKLDLK**	28.99	0/0	189597	20 + 10	1 x 20000
FAQ-$(LDLK)_3$	*FAQRVPPGGG***LDLKLDLKLDLK**	12.40	0/8	15822	8	3 x 250

Table S1. CG-MD simulations setup. $(LDLK)_3$ and FAQ-$(LDLK)_3$ SAPs aggregation propensity was evaluated through CG-MD simulations. Secondary structure (SS) parameters have been assigned according to experimental evidences; the residues with extended SS have been highlighted in bold, whereas the residues with coil SS have been highlighted in italic. The 8-mers (fibril seeds) were modeled adopting the standard MARTINI approach. The 100-mer systems was modeled adopting ONE-POT CG-MD approach [14]; the fibril seeds were modeled according to GoMARTINI mapping [10], meanwhile the monomers were mapped as used in standard MARTINI approach.

Sequence ID	Sequence	Box size (nm)	UA ions (NA+/CL-)	UA Water molecules	N° of peptides	N° of sim x time (ns)
FAQ	FAQRVPPGGG	4.0	0/1	2124	1	3 x 50
FAQ	FAQRVPPGGG	12.39	0/8	8126	8	3 x 250

Table S2. UA-MD simulations setup. FAQ functional motif self-assembling propensity was evaluated through united-atom molecular dynamics (UA-MD) simulations. Each system was represented according to Gromos53a6 force-field mapping. The peptide conformations, obtained from monomer simulations, have been used to prepare the starting configuration of 8-mer systems.

Sequence ID	Sequence	Box size (nm)	Simulation Classification	N° of peptides	N° of sim x Time (ps) x N° of seed
$(LDLK)_3$	LDLKLDLKLDLK	12.4 x 12.4 x 12.4	Axial Stretching	8	5 x 300 x 3
$(LDLK)_3$	LDLKLDLKLDLK	12.4 x 12.4 x 12.4	Bending	8	5 x 300 x 3
$(LDLK)_3$	LDLKLDLKLDLK	56.1 x 10 x 8	Axial Stretching	96	5 x 1000 x 1
$(LDLK)_3$	LDLKLDLKLDLK	28 x 30 x 8	Bending	96	5 x 1000 x 1
FAQ-$(LDLK)_3$	FAQRVPPGGGLDLKLDLKLDLK	17 x 8 x 8	Axial Stretching	8	5 x 600 x 3
FAQ-$(LDLK)_3$	FAQRVPPGGGLDLKLDLKLDLK	8 x 17 x 8	Bending	8	5 x 1000 x 3
FAQ-$(LDLK)_3$	FAQRVPPGGGLDLKLDLKLDLK	90 x 10 x 8	Axial Stretching	96	5 x 1000 x 1
FAQ-$(LDLK)_3$	FAQRVPPGGGLDLKLDLKLDLK	45 x 45 x 8	Bending	96	5 x 2000 x 1

Table S3. UA-SMD simulations setup. The fibril seeds obtained through CG-MD simulations have been used as starting configurations of UA-SMD simulations. Each system was simulated in explicit water box and submitted to five simulations differing for the initial velocity distribution.

Sequence ID	Sequence	Box size (nm)	Simulation Classification	N° of peptides	N° of sim x Time (ps) x N° of seed
$(LDLK)_3$	**LDLKLDLKLDLK**	12.4 x 12.4 x 12.4	Axial Stretching	8	5 x 300 x 3
$(LDLK)_3$	**LDLKLDLKLDLK**	12.4 x 12.4 x 12.4	Bending	8	5 x 300 x 3
$(LDLK)_3$	*LDLKLDLKLDLK*	12.4 x 12.4 x 12.4	Axial Stretching	8	5 x 300 x 3
$(LDLK)_3$	*LDLKLDLKLDLK*	12.4 x 12.4 x 12.4	Bending	8	5 x 300 x 3
$(LDLK)_3$	**LDLKLDLKLDLK**	56.1 x 10 x 8	Axial Stretching	96	5 x 1000 x 1
$(LDLK)_3$	**LDLKLDLKLDLK**	28 x 30 x 8	Bending	96	5 x 1000 x 1
$(LDLK)_3$	*LDLKLDLKLDLK*	56.1 x 10 x 8	Axial Stretching	96	5 x 1000 x 1
$(LDLK)_3$	*LDLKLDLKLDLK*	28 x 30 x 8	Bending	96	5 x 1000 x 1
FAQ-$(LDLK)_3$	*FAQRVPPGGG***LDLKLDLKLDLK**	17 x 8 x 8	Axial Stretching	8	5 x 600 x 3
FAQ-$(LDLK)_3$	*FAQRVPPGGG***LDLKLDLKLDLK**	8 x 17 x 8	Bending	8	5 x 1000 x 3
FAQ-$(LDLK)_3$	*FAQRVPPGGG***LDLKLDLKLDLK**	90 x 10 x 8	Axial Stretching	96	5 x 1000 x 1
FAQ-$(LDLK)_3$	*FAQRVPPGGG***LDLKLDLKLDLK**	45 x 45 x 8	Bending	96	5 x 2000 x 1

Table S4. CG-SMD simulations setup. $(LDLK)_3$ and FAQ-$(LDLK)_3$ fibril (seed) mechanical features were evaluated through GoMARTINI SMD simulations. Secondary structure (SS) parameters have been assigned through DSSP algorithm or imposed as fully extended according to experimental evidences; the residues with extended SS have been highlighted in bold, whereas the residues with coil SS have been highlighted in italic.

Residue	BB atom type	SC atom type	Charge
LEU-1	P5	C1	0
ASP-2	P5	Qa	-1
LEU-3	P5	C1	0
LYS-4	P5	C3,Qd	+1
LEU-5	P5	C1	0
ASP-6	P5	Qa	-1
LEU-7	P5	C1	0
LYS-8	P5	C3,Qd	+1
LEU-9	P5	C1	0
ASP-10	P5	Qa	-1
LEU-11	P5	C1	0
LYS-12	P5	C3,Qd	+1

Table S5. GoMARTINI mapping of $(LDLK)_3$ peptides. Residue refers to amino-acid residue. BB atom type refers to the MARTINI grain type corresponding to the backbone atoms of a specific residue. SC atom type refers to the MARTINI grain type corresponding to the sidechain atoms of a specific residue. The UA backmapped fibril seed structures were analyzed with DSSP and then the SS parameters have been assigned.

Residue	BB atom type	SC atom type	Charge
LEU-1	Nda	C1	0
ASP-2	Nda	Qa	-1
LEU-3	Nda	C1	0
LYS-4	Nda	C3,Qd	+1
LEU-5	Nda	C1	0
ASP-6	Nda	Qa	-1
LEU-7	Nda	C1	0
LYS-8	Nda	C3,Qd	+1
LEU-9	Nda	C1	0
ASP-10	Nda	Qa	-1
LEU-11	Nda	C1	0
LYS-12	Nda	C3,Qd	+1

Table S6. GoMARTINI mapping of $(LDLK)_3$ peptides with full extended SS parameters. Residue refers to amino-acid residue. BB atom type refers to the MARTINI grain type associated with the backbone atoms of a specific residue. SC atom type refers to the MARTINI grain type associated with the sidechain atoms of a specific residue. The SS parameters have been assigned as fully extended.

Residue	BB atom type	SC atom type	Charge
PHE-1	P5	SC5,SC5,SC5	0
ALA-2	P4		0
GLN-3	P5	P4	0
ARG-4	P5	N0,Qd	+1
VAL-5	P5	C2	0
PRO-6	P4	C3	0
PRO-7	P4	C3	0
GLY-8	P5		0
GLY-9	P5		0
GLY-10	P5		0
LEU-11	Nda	C1	0
ASP-12	Nda	Qa	-1
LEU-13	Nda	SC1	0
LYS-14	Nda	C3,Qd	+1
LEU-15	Nda	C1	0
ASP-16	Nda	Qa	-1
LEU-17	Nda	C1	0
LYS-18	Nda	C3,Qd	+1
LEU-19	Nda	C1	0
ASP-20	Nda	Qa	-1
LEU-21	Nda	C1	0
LYS-22	Nda	C3,Qd	+1

Table S7. GoMARTINI mapping of FAQ-$(LDLK)_3$ peptides. Residue refers to amino-acid residue. BB atom type refers to the MARTINI grain type corresponding to the backbone atoms of a specific residue. SC atom type refers to the MARTINI grains type corresponding to sidechain atoms of a specific residue. The UA backmapped fibril seed structures were analyzed with STRIDE and then the secondary structures were assigned.

Seed/Fibril ID	Young's Modulus (E) [MPa]	Shear Modulus (G) [MPa]	Shear Contribution Ratio s(L)
A	500	381	2,19
A (CG - dssp)	1279	840	2,41
A (CG-Ext)	1029	532	3,06
B	781	524	1,88
B(CG-dssp)	1167	821	1,39
B (CG-Ext)	820	313	2,56
C	664	566	1,31
C (CG-dssp)	1626	907	1,47
C (CG-Ext)	737	532	1,14
Fibrils	2003	612	0,06
Fibril (CG-dssp)	6252	787	0,14
Fibrils (CG-Ext)	5110	770	0,04

Table S8. Failure classification of $(LDLK)_3$ seed and fibrils. Young's (or elastic) and shear moduli were derived considering the stress-strain curves by means of ratio between the maximum stress and the corresponding strain. The shear contribution ratio was calculated as shown in section 1.5 of Material and Methods. The shear contribution ratio, s(L), provides information about strain distribution during bending failure; if s(L) > 1, non-covalent interactions are being sheared, otherwise are stretched along their direction. In $(LDLK)_3$ SAPs supramolecular structures, shear contribution ratio points out that the bending failure mechanism are mainly affected by the geometrical features of the aggregates. Indeed, the bending failure mechanism of fibril seeds is mainly ruled by shear stress, whereas the bending failure mechanism of fibrils is mainly ruled by tensional stretching of non-covalent interactions

Seed/Fibril ID	Young's Modulus (E) [MPa]	Shear Modulus (G) [MPa]	Shear Contribution Ratio s(L)
A	701	350	2,38
A (CG - dssp)	837	331	2,45
B	823	339	0,43
B(CG-dssp)	878	539	0,29
C	706	393	2,01
C (CG-dssp)	654	299	2,12
Fibrils	3823	366	0,04
Fibril (CG-dssp)	4975	503	0,03

Table S9. Failure classification of FAQ-$(LDLK)_3$ seeds and fibrils. Young's (or elastic) and shear moduli were derived as described in Table S8, meanwhile shear contribution ratio was calculated as shown in section 1.5 of Material and Methods. In FAQ-$(LDLK)_3$ SAPs supramolecular structures, the shear contribution ratio points out that the bending failure mechanisms are mainly affected by the geometrical features of the aggregates. Indeed, the bending failure mechanism of fibril seeds is mainly ruled by shear stress, whereas the bending failure mechanism of fibrils is mainly ruled by tensional stretching of non-covalent interactions.

Seed/Fibril ID	Number of Atoms/Grains	Simulated Time (ns/day)	Simulation Setup
A	62970	14.66	Traction
A(CG)	16045	368.43	Traction
A	62970	14.65	Bending
A(CG)	16045	409.79	Bending
B	62846	14.76	Traction
B(CG)	16038	144.88	Traction
B	62846	15.22	Bending
B(CG)	16038	133.39	Bending
C	62758	12.87	Traction
C(CG)	16035	159.75	Traction
C	62758	14.73	Bending
C(CG)	16035	162.82	Bending
Fibrils	152733	6.6	Traction
Fibrils(CG)	38469	75	Traction
Fibrils	225907	4.36	Bending
Fibrils(CG)	55853	33.8	Bending

Table S10. Details of $(LDLK)_3$ SAPs SMD simulations. Simulated Time refers to the output provided from the *mdrun* program of the GROMACS software suite.

Seed/Fibril ID	Number of Atoms/Grains	Simulated Time (ns/day)	Simulation Setup
A	43098	21.34	Traction
A(CG)	11013	168.47	Traction
A	43179	21.75	Bending
A(CG)	11025	181.39	Bending
B	43118	19.73	Traction
B(CG)	11013	195.87	Traction
B	43199	22.01	Bending
B(CG)	11016	112.88	Bending
C	43118	20.90	Traction
C(CG)	11021	225.22	Traction
C	43199	19.11	Bending
C(CG)	11019	163.69	Bending
Fibrils	248294	3.70	Traction
Fibrils(CG)	58759	55.68	Traction
Fibrils	544025	1.5	Bending
Fibrils(CG)	136218	25.27	Bending

Table S11. Details of FAQ-$(LDLK)_3$ SAPs SMD simulations. Simulated Time refers to the output provided from the *mdrun* program of the GROMACS software suite.

References

1. L. Martinez, R. Andrade, E. G. Birgin, J. M. Martinez, J. Comput. Chem. 2009, 30, 2157
2. L. Monticelli, S. K. Kandasamy, X. Periole, R. G. Lanson, D. P. Tieleman, S. J. Marrink, J. Chem. Theory Comput., 2008, 4, 819
3. R. Pugliese, F. Fontana, A. Marchini, F. Gelain, Acta Biomaterialia, 2018, 66, 258-271
4. D. Van der Spoel, E. Lindhal, B. Hess, G. Groenhof, A. E. Mark, H. J. C. Berendsen, J. Comput. Chem., 26, 1701-1718
5. H. J. C. Berendsen, J. P. M. Postma, W. F. Vangusteren, A. Dinola, J. R. Haak, Journal of Chemical Physics, 1984, 81, 3684-3690
6. X. Daura, K. Gademann, B. Jaun, D. Seebach, W. F. van Gusteren, A. E. Mark, Angewadte Chemie-International Edition, 1999, 38, 236-240
7. C. Oostenbrink, A. Villa, A. E. Mark, W. F. Van Gunsteren, J. Comp. Chem., 2004, 25, 1656-1676
8. J. A. Lemkul. D. R. Bevan, J. Phys. Chem. B, 2010, 114, 1652-1660
9. T. Biagini, F. Petrizelli, M. Truglio, R. Cespa, A. Barbieri, D. Capocefalo, S. Castellana, M. Florencia Tevy, M. Carella, T. Mazza, Evolutionary Bioinformatics, 2019, 15, 1-3
10. A. B. Poma, M. Cielpak, P. E. Theodorakis, J. Chem. Theory Comput., 2017, 13, 1366-1374
11. S. Keten, Z. Xu, B. Ihle, M. J. Buheler, Nature Materials, 2010, 9, 359-367
12. G. A. A. Saracino, F. Fontana, S. Jekhmane, J. M. Silva, M. Weingarth, F. Gelain
13. Y. Wang, O. Jardetzky, Protein Science, 2002, 11, 852-861
14. L. Xu, Y. Chen, X. Wang, J. Phys. Chem. B, 2014, 118, 9238-9246